Analysis and Characterization of Laterally Induced Electrostatic Repulsive Forces

Ki Bang Lee and Young-Ho Cho

Micromachines and Microsystems Laboratory
Korea Advanced Institute of Science and Technology
ME3038, Taejon 305-701, Republic of Korea, mems@kaist.ac.kr

ABSTRACT

We analyze and characterize the laterally induced electrostatic repulsive force generated by the in-plane asymmetry of electrostatic field. Basic concept of the electrostatic repulsive actuation is presented. Fundamental nature of the repulsive force has been characterized by the finite element analysis of the electrostatic field for varying electrode geometry. A simple analytic force curve has been derived from the fitting of the finite element results. The theoretical simulation results are compared well with the experimental values, measured from the microfabricated test structures : thereby demonstrating the validity and usefulness of the analytic formulae derived from the finite element simulation.

Keywords: Repulsive force, Electrostatic actuation, Finite element simulation, Electrostatic field.

INTRODUCTION

Recently, various kinds of electrostatic drive methods have been developed to generate the lateral motion of planar microstructures, and have included edge-drive [1], top-drive [2] and comb-drive [3] methods. Most of them, however, have utilized the *lateral attractive* forces, generated between in-plane [1,3] or out-of-plane [2] electrodes. Tang, *et al.* [4] discussed the use of the *transverse repulsive* force (i.e. the levitation force), generated among three *out-of-plane* electrodes for transverse motion control. In the previous work [5], we presented the concept of the *lateral repulsive* force, generated among three *in-plane* electrodes, and demonstrated the lateral repulsive drive of planar micromechanical structures.

In this paper, we analyze and characterize the laterally induced electrostatic repulsive force [5] generated by the asymmetry of in-plane electrostatic fields. Finite element electrostatic simulation has been performed for different electrode geometry and electrostatic drive voltage. A simple analytic equation of the electrostatic repulsive force is derived from the fitting of the finite element solutions. A set of polysilicon test structures has been designed and fabricated by a 4-mask surface-micromachining process. The experimental results, measured from the fabricated test structures, are compared with the theoretical values. Fundamental nature of the repulsive force has been characterized and discussed.

FINITE ELEMENT ANALYSIS

Figure 1 illustrates the concept of lateral repulsive force generated by the in-plane electrodes with different electrostatic potentials. The lateral repulsive force, F_r, on the movable electrode, is generated by the asymmetric electrostatic field distribution near the electrode tips when an induction voltage, V_C, is applied as shown in Fig.1.

Finite element analysis of the electrostatic field distribution has been performed by the commercial finite element tools, called Maxwell 2-D simulator. The repulsive force are obtained from the finite element results obtained for the DC bias voltage, V_{DC}, the movable electrode width, b, the inter-electrode gap, d, and r, respectively. Figure 2 shows the electrostatic field distribution near the electrodes for the case of the DC bias voltage of $V_{DC} = 100\ V$, the AC drive voltage of $V_{AC} = 0$ V, and the inter-electrode gaps of $r = d = 3\mu m$ and $b = 5\mu m$. In Fig. 2, we observe that the high asymmetry of the electrostatic field distribution is concentrated near the electrode tips.

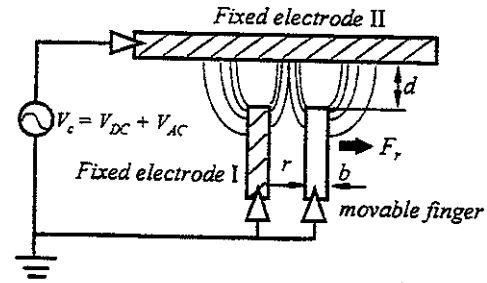

Fig.1. Working principle of a lateral repulsive-force actuation: the repulsive force, F_r, is induced by the asymmetry of the electric field when the induction voltage, V_C, is applied.

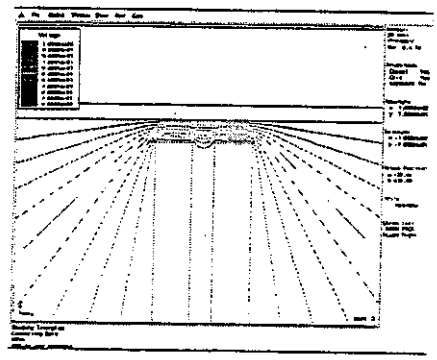

Fig.2. Finite element simulation of the electrostatic lateral force with the fixed values of V_{DC}=100V, V_{AC}=0V, r=d=3 μm and b=5μm.

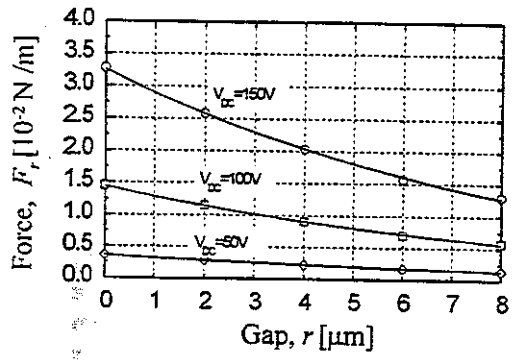

Fig. 3. Electrostatic repulsive force simulation for the varied DC bias voltage, V_{DC}, and electrode gap, r, with the fixed value of V_{AC}=0V d=3 μm and b=5μm.

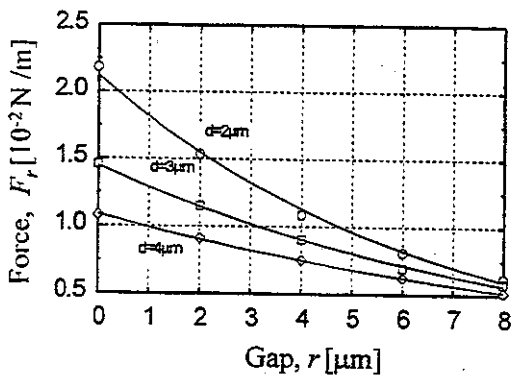

Fig. 4. Electrostatic repulsive force simulation for the varied electrode gaps, d and r, with the fixed values of V_{DC}=100V, V_{AC}=0V, and b=5μm.

Figure 3 shows the electrostatic repulsive force curves, obtained from the fitting of finite element simulation results (dotted data). From Fig. 3, we find that the repulsive force increases with the DC bias voltage, V_{DC} while the force decreases with the electrode gap, r. The greater effect of DC bias voltage is observed for the smaller gap of r. Figure 4 illustrates the dependence of the repulsive force upon the electrode gap, d. The increase of the electrode gap, d, reduces the repulsive force. The width of the movable finger causes little effect on the repulsive force, as shown in Fig.5. From the finite element solutions, we have verified that the distribution of the electrostatic field (Fig.2) is insensitive to the movable finger width, b. Judging from Figs.3, 4 and 5, we can conclude that the lateral repulsive force is highly dependent on V_{DC}, d and r rather than on b.

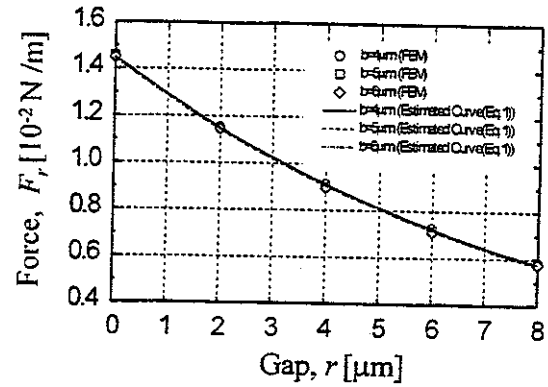

Fig. 5. Electrostatic repulsive force simulation for the varied electrode gaps, b and electrode gap, r, with the fixed values of V_{DC}=100V, V_{AC}=0V, and d=3μm.

From the fitting of the finite element solutions (the dotted data in the Figs.3, 4 and 5), we derive the lateral repulsive force per unit structure thickness, F_r, (Fig.1) in the form of:

$$F_r = A_1 e^{-\frac{r}{B}} V_c^2 \qquad (1)$$

where A_1 and B are the constants depending on the electrode geometry, r is the inter-electrode gap between the movable electrode and the fixed electrode I. From the finite element solutions for the case of b=5μm and d=3μm, we find the constants, A_1 and B, of Eq.(1) as 1.46×10^{-6} [N/mV^2] and 8.68×10^{-6} [m], respectively.

TEST STRUCTURES

Figure 6 shows the schematic drawings of the test structure, whose sizes and performances are listed in Table 1. The movable mass, suspended by the micromechanical flexures, is driven in the lateral direction (i.e. the x direction in Fig.6) by the electrostatic repulsive force, F_r. The theoretical model of the test structure can be considered as a one-degree-of freedom dynamic system,

composed of the mass, m, the stiffness, k, and the damper of a damping coefficient, c. The electrostatic drive voltage, V_C, can be expressed as the sum of the DC component of V_{DC}, and the AC component of V_{AC}. For the applied voltage of V_C , the gap, r, between the fixed electrode I and the movable electrode increases from the initial gap, r_O, to the final gap, r_1. The final gap, r_1, is obtained from the balance of the electrostatic repulsive force and the spring force generated by the flexures.

For the DC bias voltage, V_{DC}, the lateral electrostatic repulsive force, F_t, can be expressed in terms of the final gap, r_1, as follows.

$$F_t = ntF_r = Ae^{-\frac{r_1}{B}}V_{DC}^2 = k(r_1 - r_0) \quad (2)$$

where

$$A = n\,t\,A_1 \quad (2a)$$

In Eq.(2), the F_r, n, t, A_1 and r_0 denote the lateral repulsive force per unit structure thickness, the number of movable electrodes, the thickness of the test structure, the force constant of Eq.(1) and the initial gap between the fixed electrode I and the movable electrode, respectively. The k in Eq.(2) indicates the stiffness of the flexure (Fig.6).

On this basis, a set of the lateral electrostatic repulsive force test structures (Table 1) has been designed and fabricated by a 4-mask surface-micromachining process [5]. Using the Eq.(2), we can obtain the experimental values of the lateral repulsive force, F_r, from the measured values of the final gap, r_1.

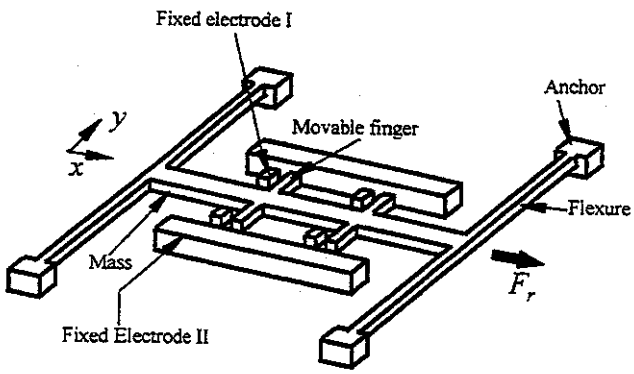

Fig. 6. Schematic diagram of the lateral repulsive force test structure: the mass and movable electrode are suspended by the flexures, driven laterally by the repulsive force, F_r, generated by the asymmetric distribution of electrostatic field among three electrodes.

Table 1. Measured dimension and estimated performance of the test structure.

dimension and performance	values
flexure width	2.8 ± 0.2 μm
mass*	0.27 ± 0.01 μg
lateral stiffness*	1.38 ± 0.3 N/m
resonant frequency	11.4 ± 1.0 kHz
initial gaps	3.0 ± 0.2 μm
number of movable electrodes	32 ea

* based on the polysilicon density of 2.33g/cm^3 and the measured Young's modulus of 100GPa.

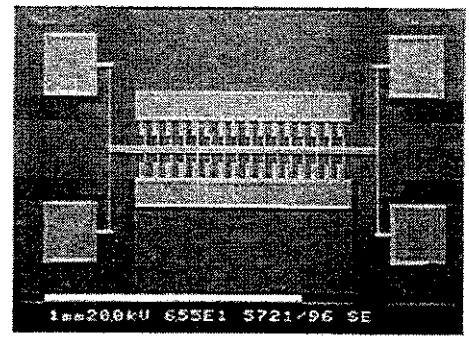

Fig.7. SEM photograph of the fabricated test structure.

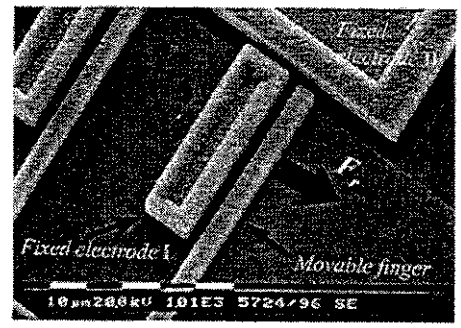

Fig. 8. Enlarged view of the fixed electrodes and the movable finger of the test structure with the sizes of r=d=3 μm and b=5μm.

RESULTS AND DISCUSSION

Figure 7 shows an SEM photograph of the fabricated test structure with an overall size of 1.5×1.0mm^2. Figure 8 is an enlarged view of the fixed electrodes and movable electrode of the fabricated test structure, shown in Fig.7.

Using the fabricated structure, a static drive test has been performed for varying DC bias voltage at the atmospheric pressure. From Eq.(2) with the measured static deflection, we obtained the lateral repulsive force, F_r.

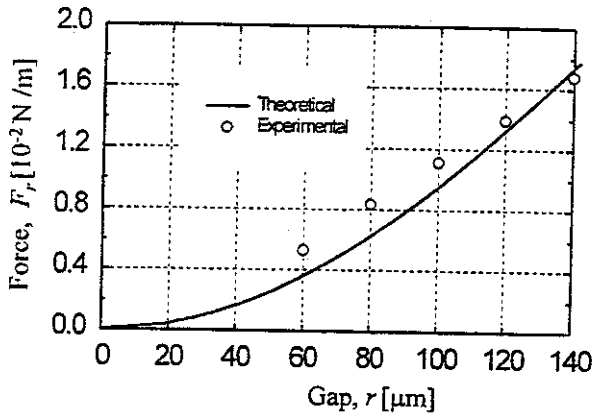

Fig. 9. Estimated and measured repulsive force from the test structure, driven by the varied DC bias voltage, V_{DC}, with no AC drive voltage, V_{AC}=0.

Figure 9 compares the estimated and measured repulsive force of the test structure with the initial gap, r_0=3μm, for the varying DC bias voltage, V_{DC}. The theoretical repulsive force in Fig.9 are estimated from the Eq.(1) with the use of the measured dimensions of Table 1 and the force constant (A_1=1.46×10^{-6}[N/m/V^2], B=8.68×10^{-6}[m]) obtained from the finite element simulation (Fig.3). The repulsive force (Fig.9) is obtained as 1.74x10^{-2} N/m from the static deflection measured at the DC bias voltage of V_{DC} =140V; while the theoretical value is estimated as 1.68x10^{-2} N/m at the DC bias voltage of V_{DC} =140V. We think that the discrepancy between the theoretically estimated values and the experimentally derived values in Fig.9 is due to the errors from the two dimensional analysis of three dimensional structures, and the levitation effect errors.

As we have expected from the theoretical analysis of Eq.(2), it is verified experimentally that the DC bias voltage of the test structure generates the repulsive force, thereby increasing the effective stiffness and the resonant frequency of the microstructure [5]; while the DC bias voltage of the conventional attractive force microactuators [3] decreases the effective stiffness and the resonant frequency. It is also observed that the movable electrode never touches the fixed electrode I for a higher voltage due to the repulsive nature of the force.

CONCLUSION

We analyze and characterize the lateral repulsive force induced by the asymmetry of the electrostatic field between a movable finger and a pair of fixed electrodes when an induction voltage is applied . From the finite element simulation, we found that the repulsive force is an exponential function of the inter-electrode gap. A set of repulsive force polysilicon test structures was designed and fabricated by a 4-mask surface-micromachining process. We verified theoretically and experimentally that the DC bias voltage increases the lateral repulsive force and the inter-electrode gap. The repulsive force of the fabricated test structure was increased with the force induction voltage. The repulsive force of 1.68x10^{-2} N/m was obtained from the microfabricated devices at the DC bias voltage of V_{DC}=140V and that of 1.74x10^{-2} N/m was estimated from the theoretical simulation. The repulsive force was increased from 0.55x10^{-2} N/m to 1.68x10^{-2} N/m for the net DC bias voltage increase of 80V from 60V, resulting in the force sensitivity of 1.4x10^{-4} N/m V. Due to the repulsive nature of the electrostatic forces, contact-free operation of microstructures was observed at the high electrostatic drive voltage.

REFERENCES

1. L.-S. Fan, Y.-C. Tai and R.S. Muller, "IC-Processed Electrostatic Micromotors," *Proc. IEDM,* San Francisco, CA, U.S.A., pp.666-669, 1988.
2. M. Mehregany, S.F. Bart, LS Tavrow, J.H. Lang, S.D. Senturia and M.F. Schlecht, "A Study of Three Microfabricated Variable-Capacitance Motors," *Sensors and Actuators*, Vol.A21-23, 173-179, 1990.
3. W. C. Tang, T.-C H. Nguyen and R. T. Howe, "Laterally Driven Polysilicon Resonant Microstructures," *Sensors and Actuators*, Vol.A20, 25-32, 1989.
4. W.C. Tang, M.G. Lim and R.T. Howe, "Electrostatic Comb Drive Levitation and Control Method," *J. Microelectromech. Sys.*, Vol.1, No.4, 170-178, 1992.
5. K.B. Lee and Y.-H. Cho, "A Lateral Repulsive-Force Drive using Asymmetric Electrostatic Field," ASME International Mechanical Engineering Congress and Exposition, Dallas, Texas, U.S.A., Nov. 1997.